

Qualification of Ti6Al4V ELI Alloy Produced by Laser Powder Bed Fusion for Biomedical Applications

I. YADROITSEV,^{1,4} P. KRAKHMALOV,² I. YADROITSAVA,¹
and A. DU PLESSIS³

1.—Department of Mechanical and Mechatronic Engineering, Central University of Technology, Free State, Bloemfontein 9300, South Africa. 2.—Department of Engineering and Physics, Karlstad University, 651 88 Karlstad, Sweden. 3.—CT Scanner Facility, University of Stellenbosch, Stellenbosch 7602, South Africa. 4.—e-mail: iyadroitsau@cut.ac.za

Rectangular Ti6Al4V extralow interstitials (ELI) samples were manufactured by laser powder bed fusion (LPBF) in vertical and horizontal orientations relative to the build platform and subjected to various heat treatments. Detailed analyses of porosity, microstructure, residual stress, tensile properties, fatigue, and fracture surfaces were performed based on x-ray micro-computed tomography, scanning electron microscopy, and x-ray diffraction methods. The types of fracture and the tensile fracture mechanisms of the LPBF Ti6Al4V ELI alloy were also studied. Detailed analysis of the microstructure and the corresponding mechanical properties were compared against standard specifications for conventional Ti6Al4V alloy for use in surgical implant applications. Conclusions regarding the mechanical properties and heat treatment of LPBF Ti6Al4V ELI for biomedical applications are made.

INTRODUCTION

The mechanical properties, heat treatments, and processing of conventional Ti6Al4V are well documented in standards for biomedical applications (ASTM F1108-14, F147208, F136-13, F620-11, ISO20160:2006) (Supplementary Fig. S1). The chemical composition requirements for additively manufactured (AM) alloys coincide with those for conventional materials (Supplementary Table SI). For wide application in the medical industry, it is crucial that laser powder bed fusion (LPBF) Ti6Al4V extralow interstitials (ELI) implants comply with international standards regarding their microstructure and mechanical properties.

This investigation is dedicated to systematic analysis of the defects, microstructure, and mechanical properties of LPBF Ti6Al4V ELI, making use of horizontal and vertical samples in as-built and heat-treated conditions. The importance of heat treatment to achieve LPBF materials with designed complex properties is also illustrated.

MATERIALS AND METHODS

Spherical argon-atomized Ti6Al4V ELI powders with the chemical compositions and size distributions indicated in Tables SI and SII were used. Vertical and horizontal rectangular blocks with dimensions of 10 mm × 10 mm × 60 mm were produced directly on Ti6Al4V substrates using an EOSINT M280 system at volume rate of 5 mm³/s for powder layer thickness of 30 μm with argon as protective atmosphere and oxygen level in the chamber of 0.07–0.12%.

The first set of as-built blocks were cut off from the substrate for further tests without heat treatment. The second and third sets of specimens remained on the substrate and were heat treated in Ar atmosphere at 650°C for stress relief, then cut off. The third set was additionally annealed in a vacuum furnace at 950°C (Supplementary Fig. S2).

Round specimens with threaded ends were machined from the rectangular blocks according to ASTM E8M standard (gauge length four times the diameter). Tensile tests were performed using an

Instron 1342 servohydraulic testing machine with clip-on extensometer of 12.5 mm under strain rate of 0.5 mm/min and 1.5 mm/min after removal of the extensometer.

To investigate defects and porosity, the samples were subjected to x-ray micro-computed tomography (microCT) with resolution of 10 μm .¹

RESULTS AND DISCUSSION

Porosity

MicroCT scans showed that the vertical and horizontal as-built LPBF samples had very low levels of porosity (0.0004% and 0.0018%, respectively). The maximum detected pore size was 205 μm (Supplementary Table SIII). The pores were fairly randomly distributed (Supplementary Figs. S3, S4).

Microstructure

In LPBF of Ti6Al4V, the material solidifies at high cooling rates (about 10^6 K/s), resulting in formation of metastable structures of α' hexagonal martensite with pronounced prior β -texturization in the building direction (Supplementary Fig. S5). Prior β -phase showed columnar growth with highly pronounced $\langle 100 \rangle$ texture, whereas the texture of the hexagonal α' phase was quite weak.² Under the present conditions, decomposition of nonequilibrium phases did not occur in the as-built and stress-relieved samples. X-ray diffraction (XRD) and transmission electron microscopy (TEM) analysis confirmed needle-like structure without any β precipitations. The thermomechanical history of LPBF Ti6Al4V also resulted in the presence of $\{1012\}$ -type twins in the as-built and stress-relieved samples. This type of twins in hexagonal close-packed (hcp) materials is often reported as tensile twins, and such twinning could be a possible mechanism for accommodation of thermal stresses during manufacturing.³

The columnar boundaries of prior β -phase were observed in as-built specimens, and all specimens after heat treatments. In the annealed specimens, they were also clearly visible, although the martensitic needle-like microstructure was decomposed (Supplementary Fig. S6). Decomposition of α' -martensite is accompanied by nucleation of fine α precipitates at martensite plate boundaries, enrichment of the surroundings with β -stabilizers, and finally, formation of equilibrium $\alpha + \beta$ phase mixture.⁴ Nuclei of equiaxial α -phase were found in globular phase enriched by α -stabilizing Al, being unevenly distributed in the microstructure. In the heat-treated specimens, no continuous alpha network at prior β -grain boundaries was found. This type of microstructure corresponds exactly to standards for biomedical applications required for annealed Ti6Al4V (ISO 20160, 2006).

Tensile Properties

Tensile tests were performed to investigate the influence of heat treatment on the mechanical characteristics of the specimens manufactured in horizontal and vertical directions. The modulus of elasticity did not vary significantly among the specimens and lay in the range of 110–119 GPa. The dispersion of data points in the tensile data around the mean value was more pronounced among the horizontal samples (Fig. 1). The as-built samples exhibited higher ultimate tensile strength (UTS) compared with the stress-relieved and annealed specimens. Higher strength and lower ductility of as-built samples can be explained by presence of residual stresses and fine martensitic structure.⁵ High strength characteristics are typical for as-built LPBF Ti6Al4V.^{2,4,6} After stress-relief heat treatment, the UTS decreased by 6–8% from the initial, as-built level. The yield strength (YS) after stress-relieving heat treatment did not change in comparison with as-built samples. Annealing led to significantly improved ductility of LPBF Ti6Al4V. Elongation at break was increased up to 20%, and reduction of area reached values above 46%. These changes in properties resulted from changes in the microstructure, which became close to conventional.

Fatigue Properties

To investigate the influence of surface roughness, heat treatment, and microstructure on the fatigue performance, three-point bending fatigue tests were carried out at room temperature. The specimen was oriented so that the top or side surface was subjected to the highest tensile stresses, while the other three surfaces were machined and ground (Table SIV). As a reference, one series of as-built horizontal specimens was tested after machining and grinding of all surfaces ($R_z \sim 5 \mu\text{m}$). Due to the limited numbers of specimens available, fatigue limit tests were not done; instead, the fatigue life of materials was estimated at one maximum stress value of 700 MPa.

The highest roughness values were measured on the side surface ($R_z \sim 120\text{--}135 \mu\text{m}$), and, accordingly, these specimens demonstrated shorter life to failure. Higher roughness implies deeper valleys on the surface, which can be interpreted as notches. Stress concentration in notches leads to accelerated crack nucleation. The top surface ($R_z \sim 30\text{--}60 \mu\text{m}$) demonstrated slightly better performance, while machined specimens ($R_z \sim 5 \mu\text{m}$) demonstrated the best performance and the highest number of cycles to failure (N). Residual stresses contributed substantially to fatigue life (Fig. 2). Stress relief resulted in an increase in the number of cycles to failure in vertical specimens. In the horizontal specimens, the effect was opposite, and specimens after stress relief showed lower number of cycles to failure. This unexpected result is difficult to explain.

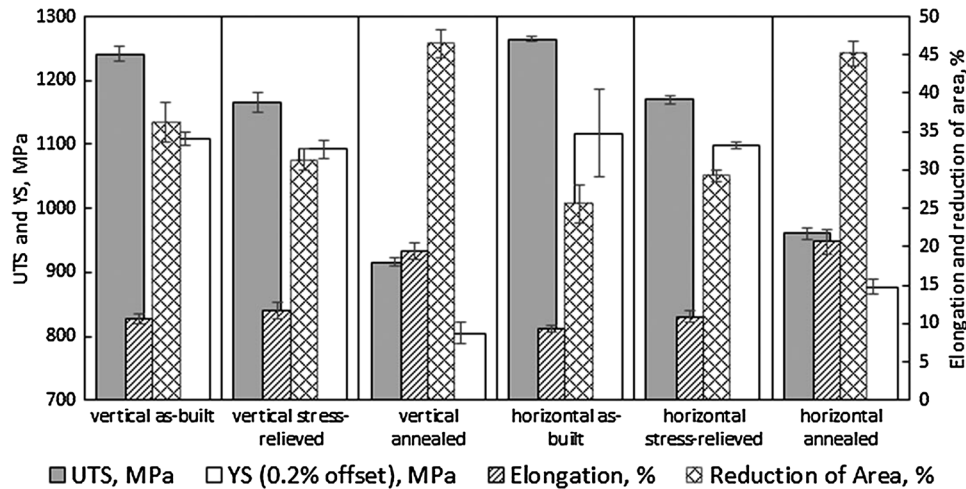


Fig. 1. Tensile mechanical properties of Ti6Al4V ELI samples.

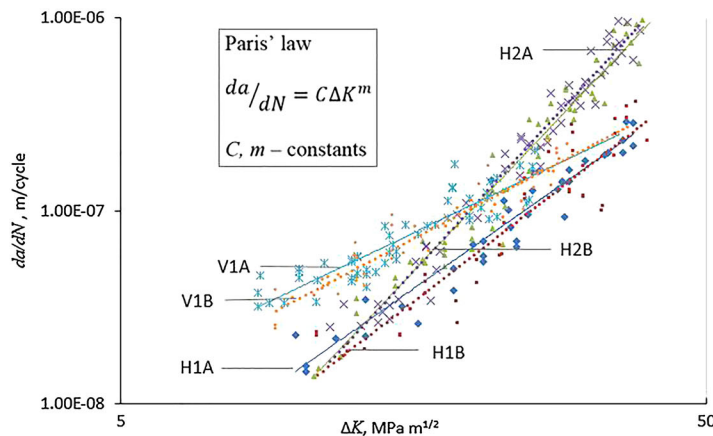


Fig. 2. Fatigue crack propagation rate and cycles to failure of LPBF Ti6Al4V ELI.

Such a decrease in the number of cycles to failure could be a result of the complex distribution of stresses in the sample.⁵ Nevertheless, this effect requires further investigation with more statistically relevant numbers of samples at different maximum stress values.

The crack propagation rate was investigated based on electron microscopy observations of striations on fracture surfaces (Fig. 2). Unlike previous reports,^{7,8} the crack penetration behavior was found to depend on specimen orientation. The influence of residual stresses on the crack propagation behavior, according to the data obtained in this study, was not great. It was observed that parameters for materials manufactured with the same orientation in as-built and stress-relieved conditions varied insignificantly.

Specimens manufactured horizontally but tested with the highest stresses at the side surface showed the steepest slope of the linear part of the da/dN curve compared with horizontal samples tested at

the top surface, or vertical specimens. These differences in crack propagation rate can be explained based on the interaction of the crack with microstructural features and interfaces in the LPBF material. For specimens manufactured horizontally and tested at the top surface, the layers have crack arrester orientation (Supplementary Table SIV). Interaction of a crack with internal interfaces can therefore result in crack deviation, thus decreasing the crack propagation rate. In horizontal specimens tested at the side surface, layers have crack divider orientation, therefore resisting crack growth more efficiently. The lowest crack propagation rate was observed for vertical specimens, for which interlayer interfaces were in-plane with the crack growth direction.

This behavior can be explained by assuming that column boundaries of prior β -phase also resist crack propagation. In the horizontal specimens, the resistance of these boundaries is not very high, as the crack grows along boundaries. Therefore, interlayer

boundaries are more important in specimens tested with this orientation. In vertical specimens, the crack penetrates perpendicularly to the boundaries of columnar prior β -grains. In these specimens, the m value is the lowest; i.e., the crack propagation rate is also low. These specimens showed the lowest number of cycles to failure, and the observed crack before the final failure occurred was shorter compared with the horizontally manufactured specimens. Thus, prior β -grain boundaries seem to be efficient in terms of resistance to fatigue crack propagation, but the material showed the lowest fatigue life.

Fracture Surface Analysis

The fracture surfaces after tensile testing of specimens in as-built, stress-relieved, and annealed conditions showed cup-and-cone shapes and obvious necking. In the annealed samples, necking was more pronounced. Necking is commonly associated with ductile fracture. The central area, commonly described as a region of fibrous fracture, was clearly distinguished, apart from the shear lips on the periphery. The surface in the fibrous zone was irregular (Supplementary Fig. S7). SEM analysis revealed formation of dimples, suggesting dimpled rupture fracture in the fibrous zone. Although dimpled rupture was dominant, quasi-cleavage facets were observed on both as-built and stress-relieved samples. Analysis at high magnification revealed martensite needles on the quasi-cleavage surfaces of the as-built and stress-relieved samples, confirming that these regions formed when the crack propagated along a martensite colony. When the crack reached a primary β -grain boundary or fusion boundary, the growth direction changed. The interface therefore acted as a crack deflector, preventing quick failure. This conclusion agrees with results presented in Ref. 9. In annealed samples, features of brittle fracture such as quasi-cleavage surfaces were not found. The dimples from the inner fracture zone were more pronounced, with larger size and shape elongated in the direction of the load.

Cup-and-cone morphology is typical for fracture controlled by pore coalescence mechanisms. The process of pore formation and coalescence was investigated by means of micro-computed tomography. The as-built and stress-relieved specimens were prestrained to 1.57–9.44%, and the pore sizes were investigated. MicroCT scans showed pore coalescence under loading in the prestrained samples; these pores looked like agglomerates of several pores (Fig. 3a). Some pores were interconnected via quite thin channels, possibly representing the initial stage of formation of cracks or new pores. As the specimen was strained, pore coarsening became clearly pronounced and became dominant in the necking area (Fig. 3b). The number of pores identified by microCT scans significantly increased in this region. Analysis of the cumulative frequency

distributions of equivalent pore diameters in prestrained, as-built, and stress-relieved samples revealed that pores became larger with increasing strain. Most of the new pores were observed in the neck region, and they act as nucleation points for cracks, leading to final failure.^{3,10}

Influence of Microstructure on Fracture Mode

To observe the influence of building direction, i.e., microstructure and orientation of prior β -grains, on the mechanical behavior of LPBF Ti6Al4V, longitudinal cross-sections of broken samples were investigated. In the horizontal specimens, two cross-sections were made, one along and one across the building direction. In all specimens, narrowing and elongation of prior β -grains was observed in the neck region.

In the horizontal specimens that were tested perpendicular to the building direction, a crack grew rather in intergranular mode, following the boundaries of prior β -columns. Crack propagation was observed along the boundaries of prior β -columns and also through the columnar grains, apparently parallel to the lamellae visible in the microstructure (Supplementary Fig. S8a, b). The presence of the mixed fracture mode could explain the experimental observation of quasi-cleavage and dimpled fracture modes simultaneously. In the vertical specimens, only intragranular fracture was observed in the cross-sections (Supplementary Fig. S8c). Grain boundaries represent weak points in the microstructure where cracks can propagate more easily.² Apparently, the presence of long prior β -grain boundaries perpendicular to the loading direction could be the reason for the lower ductility observed experimentally for the horizontal specimens.

After stress relief, there were no differences in mechanical properties among the vertical and horizontal samples. The mixed fracture mode was observed for horizontal specimens (Supplementary Fig. S9), similar to the case of as-built samples. Narrowing and elongation of prior β -grains in a stress-relieved vertical sample is presented in Fig. S9b.

Heat treatment at 950°C led to changes in the microstructure and mechanical properties. Martensitic needle-like structure transformed to α -phase lamellae with some β -phase. Only very small ($\sim 0.5 \mu\text{m}$) globular grains of α -phase were found after stress relief.³ It is notable that, after annealing, prior β -phase columns boundaries were still recognizable in the microstructure (Supplementary Fig. S6). After loading of heat-treated specimens, no indication of brittleness was observed at the fracture surface and grains were well plastically deformed (Supplementary Fig. S10). The results of the fracture surface analysis allow speculation that crack propagation occurred along α -lamellae or α - β interfaces. The influence of prior β -grain boundaries was not as great as was observed for the horizontal as-built specimens.

Qualification of Ti6Al4V ELI Alloy Produced by Laser Powder Bed Fusion for Biomedical Applications

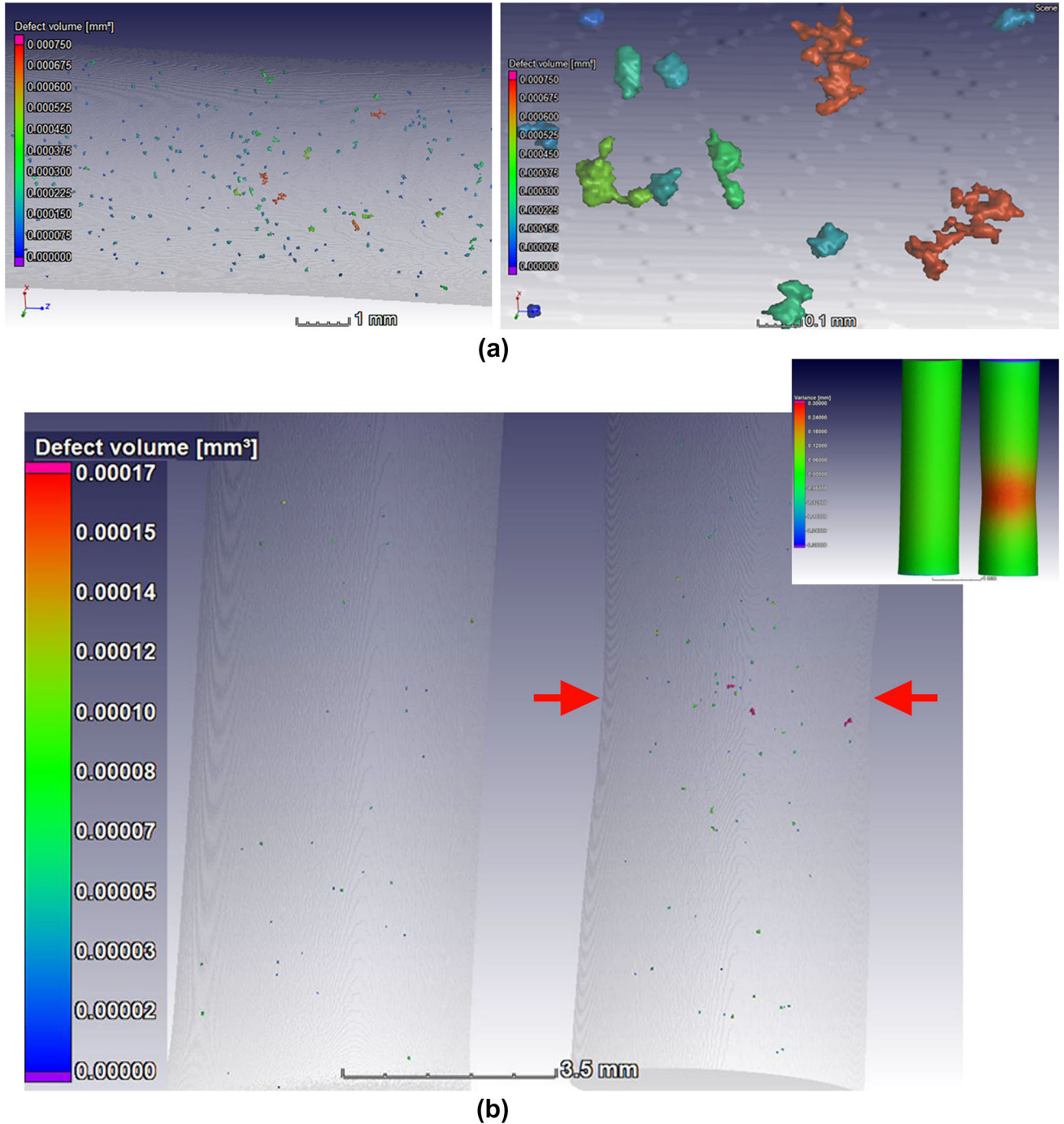


Fig. 3. Reconstruction of porosity in as-built sample deformed to 8.2% from initial length (a) and necking creation in stress-relieved sample deformed from 3.55% to 9.44% from initial length (b). Defect analysis shows color-coded porosity distribution in transparent three-dimensional (3D) views. Inset shows colour-coded thickness variation, clearly indicating the necking region.

Observation of cross-sections near the neck region in as-built specimens and after heat treatments revealed that nucleation and coalescence of pores was the main mechanism governing the failure under tension. Pores observed in the as-built and stress-relieved materials were elongated and mostly located between α' -martensite needles or on colony boundaries (Supplementary Figs. S8, S9). Stress

relief did not change the pore nucleation sites; therefore, it is possible to conclude that the pore coalescence was related to anisotropy in the microstructure. In the annealed material, pores nucleated at α -lamella boundaries and grew under tension (Supplementary Fig. S10). These microscopy observations are in very good agreement with the microCT investigations described above. It was

not the pores existing in the materials after manufacturing that resulted in the final failure; rather, new pores nucleated, grew, and coalesced to create the final crack that led to failure.

CONCLUSION

Using LPBF, high density can be achieved by choosing optimal process parameters and scanning strategy. In the present study, for Ti6Al4V ELI samples, the density measured by microCT was above 99.99% (for pores $> 30 \mu\text{m}$). The typical pore size in as-built material ranged from $30 \mu\text{m}$ to $200 \mu\text{m}$. MicroCT scans and cross-sectioning microscopic analysis revealed that the largest pores were predominantly elongated in shape and could be considered as interlayer pores.

LPBF manufacturing leads to high residual stresses in as-built objects and unique microstructure due to high cooling rates. Ti6Al4V ELI as-built microstructure consisted of hexagonal α' martensitic needles. No β precipitations were found in the as-built samples or after stress-relief heat treatment. Annealing resulted in decomposition of α' martensite and transformed the microstructure to $\alpha + \beta$ phase mixture with small equiaxial grains of α phase randomly distributed in the volume.

As-built samples fabricated in vertical and horizontal directions showed high strength ($\sim 1250 \text{ MPa}$) and relatively low ductility ($\sim 10\%$) due to the presence of residual stresses and very fine martensitic structure. After stress-relief heat treatment, the UTS decreased by 6–8% while the YTS remained unchanged. Annealing led to a significant improvement in the ductility; the elongation of break increased up to 20%. The modulus of elasticity varied insignificantly, ranging from 110 GPa to 119 GPa.

Investigations on the development of the porosity in as-built and heat-treated samples using interrupted tensile tests revealed that nucleation and coalescence of new pores, instead of growth of existing pores in the necking region, was the main mechanism causing fracture.

The bending fatigue properties of horizontal specimens revealed a correlation between the number of cycles to failure and the surface roughness. Specimens with rougher surface demonstrated decreased number of cycles to failure. The crack propagation rate was found to depend on the specimen orientation but insignificantly on residual stresses.

Cup-and-cone fracture was observed in specimens in as-built, stress-relieved, and heat-treated conditions. A mixed fracture mode with features of ductile dimpled rupture and brittle quasi-cleavage surfaces was found in as-built and stress-relieved samples. In annealed condition, the fracture mode was ductile.

Analysis of the influence of the building direction on the fracture modes showed that, in horizontal specimens, intergranular (along prior β -grain boundaries) and intragranular (along lamellae in a colony) fracture occurred. In vertical samples, only intragranular type of fracture was found. Boundaries of prior β -grains initiating intergranular fracture could therefore be a reason for the decreased ductility observed in tension tests of horizontal specimens.

LPBF Ti6Al4V ELI has a specific microstructure and mechanical properties, which are comparable or even superior to those of conventional material. Thus, there is a clear need to accelerate the development of new standards to provide clear quality indicators for use of this type of material in biomedical applications.

ACKNOWLEDGEMENTS

This work is based on research supported by the South African Research Chairs Initiative of the Department of Science and Technology and National Research Foundation of South Africa (Grant No. 97994) and the Collaborative Program in Additive Manufacturing (Contract No. CSIR-NLC-CPAM-15-MOA-CUT-01).

ELECTRONIC SUPPLEMENTARY MATERIAL

The online version of this article (<https://doi.org/10.1007/s11837-017-2655-5>) contains supplementary material, which is available to authorized users.

REFERENCES

1. A. du Plessis, S.G. le Roux, and A. Guelpa, *Nucl. Instrum. Methods B* 384, 42 (2016).
2. M. Simonelli, *Microstructure Evolution and Mechanical Properties of Selective Laser Melted Ti-6Al-4V*, PhD thesis (Loughborough University, UK, 2014).
3. P. Krakhmalev, G. Fredriksson, I. Yadroitsava, N. Kazantseva, A. du Plessis, and I. Yadroitsev, *Phys. Procedia* 83, 778 (2016).
4. F.X.G. Mur, D. Rodriguez, and J.A. Planell, *J. Alloys Compd.* 234, 287 (1996).
5. I. Yadroitsava, S. Grewar, D. Hattingh, and I. Yadroitsev, *Mater. Sci. Forum* 828–829, 305 (2015).
6. H.K. Rafi, N.V. Karthik, H. Gong, T.L. Starr, and B.E. Stucker, *J. Mater. Eng. Perform.* 22, 3873 (2015).
7. P. Edwards and M. Ramulu, *Fatig. Fract. Eng. Mater. Struct.* 38, 1228 (2015).
8. N.M. Dhansay, R. Tait, and T. Becker, *Adv. Mater. Res.* 1019, 248 (2014).
9. S. Wen, S. Li, Q. Wei, C. Yan, S. Zhang, and Y. Shi, *J. Mater. Process. Technol.* 214, 2660 (2014).
10. M.G. Moletsane, P. Krakhmalev, N. Kazantseva, A. du Plessis, I. Yadroitsava, I. Yadroitsev, *S. Afr. J. Ind. Eng.* 27, 110 (2016).